sciendo

Power Electronics and Drives
Volume 10(45), 2025 DOI: 10.2478/pead-2025-0004

Power Electronics and Drives

Robust Adaptive Control of Dual Active Bridge DC-DC Converter with Constant Power Loading

Research paper

Emmanuel K. Effah[1,2,*], Francis B. Effah[2], Philip Y. Okyere[2], Emmanuel K. Anto[2]

[1]*Ghana Communication Technology University, Accra, Ghana*
[2]*Kwame Nkrumah University of Science and Technology, Kumasi, Ghana*

Received: 06 November 2024; Accepted: 15 January 2025

Abstract: The standard model reference adaptive control (MRAC) application to the Dual Active Bridge (DAB) converter has proven to achieve excellent dynamic and tracking responses under parametric uncertainty. However, it is sensitive to bounded non-parametric uncertainty caused by measurement noise and ripples in the output voltage produced in the electronic device. When left unchecked, it affects the system's performance and may lead to instability. This paper investigates two robust modifications to the standard MRAC, namely the projection operator and dead zone techniques, to tackle the issue of the bounded noise to the dual active bridge with constant power loading (CPL). It further develops an improved form of the dead zone-based MRAC, which ensures better transient and steady-state output voltage when compared with the traditional dead-zone-based MRAC.

Keywords: *Dual Active Bridge Converter • Constant Power Loading • Dead Zone • Projection Operator • Model Reference Adaptive Control*

1. Introduction

The DC microgrid has gained attention recently, and it is set to be indispensable in future power systems due to the strong advocacy for the high penetration of renewable energy sources backing this system's excellent characteristics and accrued benefits it presents. Some of these include seamless integration of renewable energy sources, better compliance with consumer electronics, higher efficiency, the possibility of a bidirectional power flow etc.(Shao *et al.*, 2022; Meng *et al.*, 2023; Effah *et al.*, 2024). These benefits, however, come with some disadvantages. The key among them is the issue of constant power loading (CPL), which is the negative incremental impedance exhibited by the DC microgrid system, which results from its architecture where power electronic devices precede loads. The devastating effect of the CPL is that it reduces the damping of the output voltage and, in extreme cases, causes instability. In the literature, many approaches have been proffered to tackle this limitation. Some approaches use passive elements while others apply control systems. In the case of passive elements, resistances, capacitances, inductances, and a combination of same are introduced into the system to counteract the CPL. While simple, this method introduces undesirable power losses into the system, and impacts the system's size, weight, and cost. On the other hand, literature on the active systems approach has assessed the effects of introducing an active damping system involving virtual passive elements to mitigate the undesirable effects of the CPL. For example, (Rahimi and Emadi, 2009; Wu and Lu, 2015; Iyer, Gulur and Bhattacharya, 2019) have proposed a virtual resistance-based active damping scheme for tackling the CPL, (Iyer, Gulur and Bhattacharya, 2019) additionally providing a comprehensive stability assessment to back its claims. However, this approach has been found to degrade power quality. Linear and nonlinear controllers have also been introduced to tackle the voltage stability issue. Among the combination of control strategies and power converters, the control strategies applied to the dual active bridge (DAB) have received great attention recently. This is due to the excellent properties of the DAB including permission of

* *Email: eeffah@gctu.edu.gh*

Open Access. © 2025 Effah et al., published by Sciendo. (cc) BY This is an open access article licensed under the Creative Commons Attribution License (http://creativecommons.org/licenses/by/4.0/).

bidirectional flow of power, ensuring natural zero voltage switching and accommodation of wide voltage variations, establishing it to be a critical component to ensuring voltage stability of the DC bus and ensuring normal operation compared to the other traditional dc-dc converters. Linear controllers applied to DAB to ensure voltage stability in the literature, ensure stability and good tracking performance at a specific operating point, beyond which controller performance degrades. Nonlinear controllers have been proposed to ensure performance beyond this operating point. The moving discretised control-set-based Model predictive control (MDC-MPC) introduced by (Chen, Lin, *et al.*, 2020; Chen, Shao, *et al.*, 2020; Xiao *et al.*, 2020) uses the principle of optimal control to predict the best discretised phase shift ratio which ensures that a given performance index is achieved under given constraints. While results show excellent performance of the controller in terms of voltage regulation and transients, literature also shows its effectiveness is very much affected when there is a variation in parameters between the real plant and the model used in the MDC-MPC control system. As proposed by (Jeung and Lee, 2019) the double integral sliding mode control shows excellent robust performance. Still, the steady-state performance is less desirable due to the chattering nature of the control system output.

Model reference adaptive control (MRAC) is another advanced nonlinear control method known for its strong dynamic and steady performance under parametric variation and disturbances (Brando, Del Pizzo and Meo, 2018; Effah *et al.*, 2024). Previous work, such as (Effah *et al.*, 2024), applied the standard MRAC considering CPL conditions; however, this approach is criticized for its sensitivity to bounded non-parametric uncertainties, including measurement noise and voltage ripples from the electronic devices, which can degrade performance and risk system instability. This paper addresses these limitations by implementing projection operator and dead zone methods on the standard MRAC to manage the bounded non-parametric noise and ripples within the DAB under CPL. Theoretical analyses substantiate the instability risks posed by such non-parametric uncertainties, and simulations show that both the projection operator and dead zone based MRAC methods mitigate parameter drift, thus ensuring robustness. Additionally, simulations demonstrate that the dead zone approach offers superior performance over the projection operator method for power electronic applications. Again, a refined dead zone based MRAC is proposed, yielding further improvements in both transient and steady-state response, thereby advancing robust MRAC capabilities.

The rest of the paper is summarized as follows: Section 2 models the DAB with CPL, Section 3 introduces the concept and effect of bounded non-parametric uncertainties, stability analysis and the design of Robust MRAC based on dead zone and projection operator techniques. Section 4 provides simulation results and analysis, and Section 5 concludes the paper.

2. Modelling of DAB with CPL

Modelling is essential in producing effective control strategies for many physical systems. The reduced order model, extended state space average model, and discrete-time model are power converter modelling techniques in the literature (Shah and Bhattacharya, 2017; Mueller and Kimball, 2018; Iqbal *et al.*, 2020). A comprehensive comparison of the different models, considering aspects such as complexity and accuracy under both small and large disturbances, demonstrated that the reduced order model of the DAB stands out as the best (Shao *et al.*, 2022; He *et al.*, 2023). Thus, in this paper, the reduced order model is used to develop the DAB with CPL. Additionally, the Single-phase shift (SPS) modulation technique is chosen since it is more widely used in today's industry than other advanced modulation techniques. (He *et al.*, 2023)

Figure 1 shows the general SPS based DAB circuit, connected to both a load resistor and CPL. In this setup, v_1, i_{b1}, v_2 and i_{b2} represent the DAB's input voltage, input current, output voltage, and output current, respectively, with C_1 and C_2 indicating the input and output capacitances. The high-frequency isolation transformer has a primary to secondary turns ratio *N*. S_x (where $x = 1-8$) represents an insulated gate bipolar transistor (IGBT) connected to antiparallel diodes. The IGBT are subjected to the control signal to produce voltages v_{ab} and v_{cd}. In the production of voltage v_{ab} at the primary side of the high frequency transformer, the control signals of the pair S_1 and S_4 must be identical and that of S_2 and S_3 must also be identical. However, the two pairs must be complementary 50% duty cycle signals. At the secondary side of the transformer, v_{cd} is produced using a similar approach: the pair (S_5, S_8) is subjected to the same control signal of 50% duty cycle and the pair (S_6, S_7) is subjected to another control signal which is complementary to that of the pair (S_5, S_8). The control signals of the secondary bridge replicate those of the primary bridge, albeit with a phase shift d. Therefore v_{ab} and v_{cd} can have only two states, (positive and

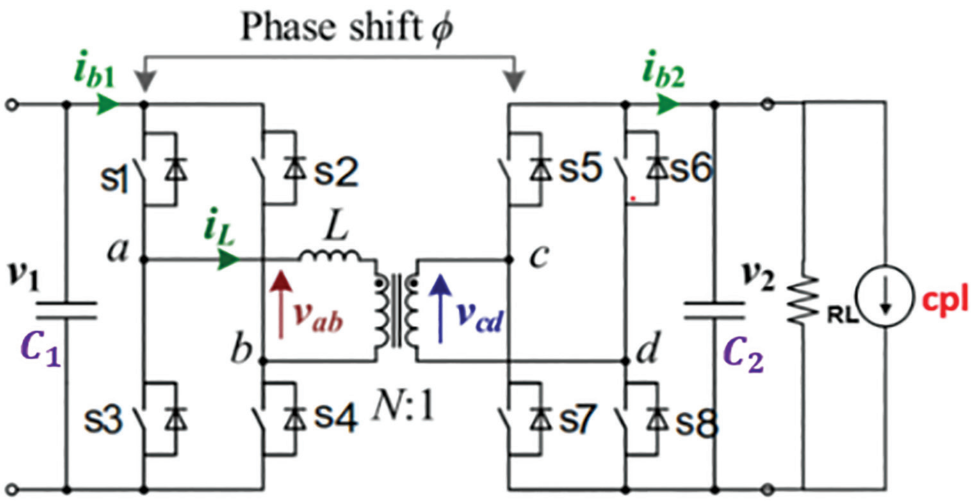

Figure 1. Topology of DAB connected with CPL.

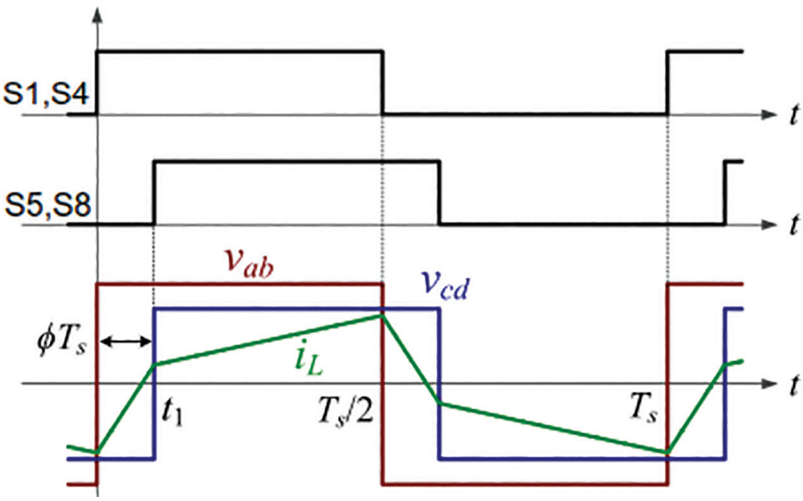

Figure 2. SPS modulation and associated current and voltage.

negative) as shown in Figure 2. Figure 3 also shows the input and output current waveforms produced. The voltage waveforms in Figure 2, the rectified inductor current waveform (Figure 3) and the principle that the rate of change of inductor current is proportional to the ratio of the total voltage across it to its inductance $\left(\frac{di_L}{dt}=\frac{v_L}{L}\right)$ can then be used in deriving the output power in equation (1). Analysis of half of the period suffices as the DAB has symmetric characteristics. The output power equation of the SPS modulated DAB can be expressed (Shao *et al.*, 2022)

$$P_{out} = \frac{Nv_1v_2d(1-2d)}{f_sL} \tag{1}$$

P_{out} = output power, N = turns ratio of the transformer, f_s = switching frequency of DAB, d = phase shift ratio.

The average output current $\langle i_{b2} \rangle$ is determined from P_{out}. This is achieved by making $\langle i_{b2} \rangle$ the subject of the equation $P_{out} = v_2 \langle i_{b2} \rangle$.

At the output end, the DAB is connected to the load resistor representing a constant voltage source and the CPL, which is approximated by its first order Taylor series model as shown in equation (2). It is assumed that the

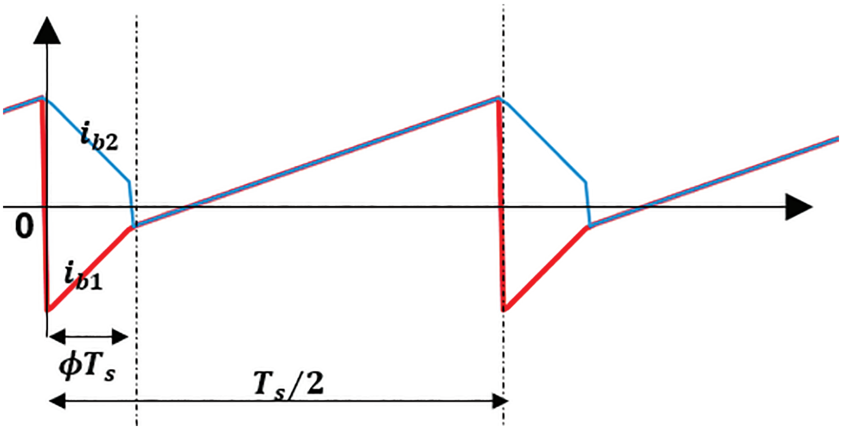

Figure 3. Input and output current waveforms.

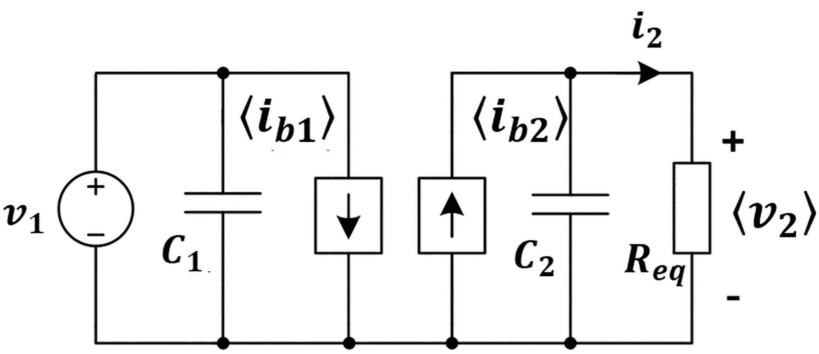

Figure 4. Reduced order model of the DAB.

CPL dominates hence further analysis would consider only CPL. The Kirchhoff's current law is applied on the reduced order model of the DAB in Figure 4. The state equation of the reduced order DAB with CPL is provided in equation (3) Please note that $\langle v_2 \rangle$ is the average value of the output voltage v_2 in a switching period.

$$\begin{aligned} i_2 &= 2\frac{P_{cpl}}{V_2} - \frac{P_{cpl}}{V_2^2} v_2 \\ &= 2\frac{P_{cpl}}{V_2} - \frac{1}{R_{eq}} v_2 \end{aligned} \tag{2}$$

Where P_{cpl}, V_2 are the power of CPL and value of v_2 at a given operating point respectively

$$\begin{aligned} \frac{d\langle v_2 \rangle}{dt} &= -\frac{\langle v_2 \rangle}{\mathrm{R}_{eq} C_2} + \frac{N v_1 (1-2d)d}{f_s L C_2} \\ \dot{x} &= -a_p x + b_p u \\ a_p &= \frac{1}{\mathrm{R}_{eq} C_2}, b_p = \frac{N v_1}{f_s L C_2}, u = (1-2d)d, x = \langle v_2 \rangle \end{aligned} \tag{3}$$

3. Stability issues and design of Robust Adaptive Controller

This section begins with an introduction to MRAC, then proceeds to show the impact unmodelled parameter uncertainties has on the stability of the DAB system and how the dead zone and projection operator techniques address it. Finally, a Robust MRAC is designed for the DAB control system.

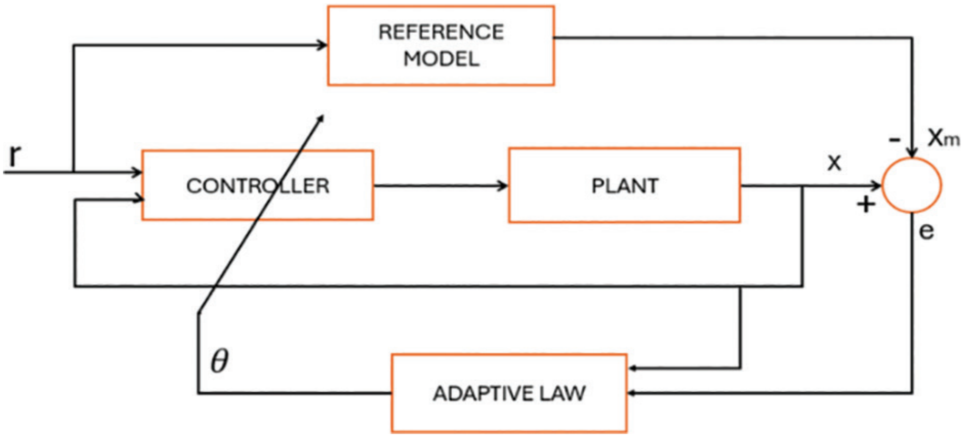

Figure 5. General structure of MRAC control system.

The model reference adaptive control (MRAC) is one of the variants of adaptive control. The general structure of the MRAC is as shown in Figure 5. The reference model is chosen to generate the desired trajectory (x_m) for the plant output (x) to replicate. The tracking error (*e*) serves as the input to an online adaptive mechanism. This then feeds the controller with appropriate control laws to ensure that the tracking error is zero. MRAC has proven useful for applications where the plant structure is known but its parameters are uncertain.

Assessing the impact of non-parametric uncertainties starts with selecting a reference model for the MRAC which takes a first order system structure as shown in equation (4). The choice of the order is due to the fact that our reduced order model is also a first order system

$$\begin{aligned} \dot{x}_m &= -a_m x_m + b_m r \\ a_m &> 0 \\ x_m(0) &= x_{m0} \end{aligned} \tag{4}$$

In equation (4) the value of a_m is chosen such that the reference model is Hurwitz and Strictly Positive Real (SPR). Equation (3) is parameterised by adding and subtracting $a_m x$ giving rise to equation (5)

$$x = \frac{1}{s + a_m}\left(b_p u - \left(a_p - a_m\right)x\right) \tag{5}$$

Let, $\theta_1 = b_p, \theta_2 = -\left(a_p - a_m\right), \omega_1 = \frac{u}{s + a_m}, \omega_2 = \frac{x}{s + a_m}$ where s is the Laplace transform variable. Then,

$$x = \theta_1\omega_1 + \theta_2\omega_2 \tag{6}$$

With the assumption that the output can be represented as equation (6) and applying the certainty equivalence principle, the unknown parameters θ_1 and θ_2 can be replaced by their estimates $\hat{\theta}_1$ and $\hat{\theta}_2$, hence the adaptive laws can be determined as follows:

$\dot{\hat{\theta}}_1 = \lambda_1\varepsilon\omega_1$ and $\dot{\hat{\theta}}_2 = \lambda_2\varepsilon\omega_2$ where $\varepsilon = x - \left(\hat{\theta}_1\omega_1 + \hat{\theta}_2\omega_2\right)$; that is the difference between the actual and the estimated parameter values.

To investigate the boundedness and convergence of the estimated parameters, equation (6) assumes the Lyapunov candidate as given in equation (7) and then its derivative is further analysed in equation (8). From equation (8) Lyapunov stability has been established, showing that the boundedness of the parameter and its estimate since $\tilde{\theta}_i$ is bounded regardless of the value of ω_i.

$$\begin{aligned} V &= \frac{1}{2\lambda_1}\tilde{\theta}_1^2 + \frac{1}{2\lambda_2}\tilde{\theta}_2^2 \\ \tilde{\theta}_i &= \theta_i - \hat{\theta}_i \\ i &= 1,2 \end{aligned} \tag{7}$$

$$\begin{aligned}
\dot{V} &= \frac{\tilde{\theta}_1\dot{\tilde{\theta}}_1}{\lambda_1} + \frac{\tilde{\theta}_2\dot{\tilde{\theta}}_2}{\lambda_2} \\
\dot{V} &= -\tilde{\theta}_1\left(\varepsilon\omega_1\right) - \tilde{\theta}_2\left(\varepsilon\omega_2\right) \\
&= -\left(\tilde{\theta}_1\omega_1 + \tilde{\theta}_2\omega_2\right)^2 \\
&\le 0
\end{aligned} \tag{8}$$

However, with the introduction of the unmodelled dynamics, particularly the ripple noise which corrupts the output, $x = \theta_1\omega_1 + \theta_2\omega_2 + d(t)$ where $d(t)$ takes into account the unmodelled noise. Under this condition, the derivative of the Lyapunov candidate is analyzed as follows:

$$\begin{aligned}
\dot{V} &= -\left(\tilde{\theta}_1\omega_1 + \tilde{\theta}_2\omega_2\right)\varepsilon \\
&= -\left(\tilde{\theta}_1\omega_1 + \tilde{\theta}_2\omega_2\right)\left(\tilde{\theta}_1\omega_1 + \tilde{\theta}_2\omega_2 + d(t)\right) \\
&= -\left(\left(\tilde{\theta}_1\omega_1 + \tilde{\theta}_2\omega_2\right)^2 + d(t)\left(\tilde{\theta}_1\omega_1 + \tilde{\theta}_2\omega_2\right)\right) \\
&= -\frac{\left(\tilde{\theta}_1\omega_1 + \tilde{\theta}_2\omega_2\right)^2}{2} - \frac{\left(\tilde{\theta}_1\omega_1 + \tilde{\theta}_2\omega_2 + d(t)\right)^2}{2} + \frac{d(t)^2}{2}
\end{aligned} \tag{9}$$

From equation (9), we cannot conclude the boundedness of $\tilde{\theta}_i$ even though ω_i is bounded. A good example of this result is shown in (Ding, 2013), who corroborates the notion that the unmodelled noise can cause parametric drift and if not adequately addressed could lead to instability. The next paragraphs provide two modifications namely the dead zone and the projection operator in redesigning the adaptive laws to address the parameter drift.

The dead zone technique is a modification to the parameter adaptive law to stop parameter adaption when the error is very close to zero. The adaptive law is thus modified as in equation (10), where c is the constant satisfying $c > \left|d(t)\right|$ for all t.

$$\dot{\hat{\theta}}_i = \begin{cases} \lambda_i\varepsilon\omega_i & |\varepsilon| > c \\ 0 & |\varepsilon| \le c \end{cases} \qquad i = 1,2 \tag{10}$$

As an example, for $\varepsilon > c$

$$\begin{aligned}
\dot{V} &= -\left(\tilde{\theta}_1\omega_1 + \tilde{\theta}_2\omega_2\right)\varepsilon \\
&= -\left(\theta_1\omega_1 - \hat{\theta}_1\omega_1 + \theta_2\omega_2 - \hat{\theta}_2\omega_2\right)\varepsilon \\
&= -\left(x - d(t) - \hat{\theta}_1\omega_1 - \hat{\theta}_2\omega_2\right)\varepsilon \\
&= -\left(\varepsilon - d(t)\right)\varepsilon \\
&< 0
\end{aligned} \tag{11}$$

In contrast, the projection operator employs the gradient projection method to ensure that the parameter estimates consistently remain within a limited convex set in the parameter space. We want to limit $\hat{\theta}_i$ to lie inside the convex bounded set $g_i\left(\hat{\theta}_i\right) \triangleq \left\{\hat{\theta}_i \mid \hat{\theta}_i^2 \le r_i^2\right\}$. Assuming that the unmodeled ripple/ noise is upper bounded by the value d_o, the projection operator based MRAC is designed in equation (12)

$$\dot{\hat{\theta}}_i = \begin{cases} \lambda_i\varepsilon\omega_i & if \left|\hat{\theta}_i\right| < r_i, if \left|\hat{\theta}_i\right| = r_i \ and \ \hat{\theta}_i\varepsilon\omega_i \le 0 \\ 0 & if \left|\hat{\theta}_i\right| = r_i \ and \ \hat{\theta}_i\varepsilon\omega_i > 0 \end{cases} \qquad i = 1,2 \tag{12}$$

For the case where $\dot{V}=0, \left|\hat{\theta}_i\right|=r_i$ and $\hat{\theta}_i\varepsilon\omega_i>0$ we have

$$\begin{aligned}\dot{V}&=\tilde{\theta}_1\left(\varepsilon\omega_1-\varepsilon\omega_1\right)+\tilde{\theta}_2\left(\varepsilon\omega_2-\varepsilon\omega_2\right)\\&=\left(\tilde{\theta}_1\varepsilon\omega_1+\tilde{\theta}_2\varepsilon\omega_2\right)-\left(\tilde{\theta}_1\varepsilon\omega_1+\tilde{\theta}_2\varepsilon\omega_2\right)\\&=-\varepsilon^2+d\left(t\right)\varepsilon-\left(\tilde{\theta}_1\varepsilon\omega_1+\tilde{\theta}_2\varepsilon\omega_2\right)\end{aligned}$$

The last term in the equation of $\dot{V}$ can be written as

$$\begin{aligned}\left(\tilde{\theta}_1\varepsilon\omega_1+\tilde{\theta}_2\varepsilon\omega_2\right)&=\left(\hat{\theta}_1\varepsilon\omega_1+\hat{\theta}_2\varepsilon\omega_2\right)-\left(\theta_1\varepsilon\omega_1+\theta_2\varepsilon\omega_2\right)\\&=\left(r_1\,sgn\left(\hat{\theta}_1\right)\varepsilon\omega_1+r_2\,sgn\left(\hat{\theta}_2\right)\varepsilon\omega_2\right)-\left(\theta_1\varepsilon\omega_1+\theta_2\varepsilon\omega_2\right)\end{aligned}$$

Therefore for $\hat{\theta}_1\varepsilon\omega_1>0, \hat{\theta}_2\varepsilon\omega_2>0$ and $\left|\hat{\theta}_1\right|=r_1, \left|\hat{\theta}_2\right|=r_2$ we obtain,

$$\begin{aligned}&\tilde{\theta}_1\varepsilon\omega_1=r_1\left|\varepsilon\omega_1\right|-\theta_1\varepsilon\omega_1\geq r_1\left|\varepsilon\omega_1\right|-\left|\theta_1\right|\left|\varepsilon\omega_1\right|\geq 0\\&\qquad\qquad and\\&\tilde{\theta}_2\varepsilon\omega_2=r_2\left|\varepsilon\omega_2\right|-\theta_2\varepsilon\omega_2\geq r_2\left|\varepsilon\omega_2\right|-\left|\theta_2\right|\left|\varepsilon\omega_2\right|\geq 0\end{aligned}$$

Where the last inequalities are obtained by assuming that $r_1\geq\left|\theta_1\right|, r_2\geq\left|\theta_2\right|$, which implies that for $\left|\hat{\theta}_i\right|=r_i$ and $\hat{\theta}_i\varepsilon\omega_i>0$ we have $\tilde{\theta}_i\varepsilon\omega_i\geq 0$ and that $\dot{V}=0\leq-\varepsilon^2+\varepsilon d\left(t\right)$. Applying the Young's inequality to the product term we obtain equation (13)

$$\dot{V}\leq-\varepsilon^2+\varepsilon d\left(t\right)\leq\frac{-\varepsilon^2}{2}+\frac{d_0}{2}, \forall t\geq 0 \tag{13}$$

A bound for ε in the mean square sense may be obtained by integrating both sides of equation (13) to get

$$\int_t^{t+T}\varepsilon^2 d\tau\leq d_o^2T+2\left(V\left(t\right)-V\left(t+T\right)\right)$$

$\forall t\geq 0$ and any $T\geq 0$. Since V is bounded, it follows that ε is also bounded.

Having presented the stability issue associated with unmodelled non-parametric uncertainties and suggested solutions from the parameter estimation-based point of view, this paragraph is dedicated to the design of the robust MRAC controller in particular. It is important to note that the robust adaptive laws derived previously are analogous to the Robust MRAC design. However, in this case we concentrate on the tracking error $\left(e\right)$ between the plant output $\left(x\right)$ and the reference model $\left(x_m\right)$ as opposed to the parametric error $\left(\varepsilon\right)$.

From equations (4) and (5) the tracking error dynamics would be as specified in equation (14)

$$\begin{aligned}&e=x-x_m\\&e\left(s+a_m\right)=b_p\left(u-\frac{b_m}{b_p}r-\frac{\left(a_p-a_m\right)}{b_p}x\right)\\&\dot{e}=-a_me+b_p\left(u-\frac{b_m}{b_p}r-\frac{\left(a_p-a_m\right)}{b_p}x\right)\\&\dot{e}=-a_me+b_p\left(u-\theta_1^*\omega_1^*-\theta_2^*\omega_2^*\right)\\&\theta_1^*=\frac{b_m}{b_p}, \theta_2^*=\frac{\left(a_p-a_m\right)}{b_p}\\&\omega_1^*=r, \omega_2^*=x\end{aligned} \tag{14}$$

With an adaptive input of $u=\hat{\theta}_1^*\omega_1^*+\hat{\theta}_2^*\omega_2^*$ the closed loop system dynamics is given as:

$$\dot{e}=-a_m e+b_p\left(-\tilde{\theta}_1^*\omega_1^*-\tilde{\theta}_2^*\omega_2^*\right)$$

where $\tilde{\theta}_1^*=\theta_1^*-\hat{\theta}_1^*$ and $\tilde{\theta}_2^*=\theta_2^*-\hat{\theta}_2^*$. From the closed loop system dynamics, we select the Lyapunov equation $V=\frac{1}{2}e^2+\frac{|b_p|}{2\lambda_1}\left(\tilde{\theta}_1^*\right)^2+\frac{|b_p|}{2\lambda_2}\left(\tilde{\theta}_2^*\right)$. The derivative of this function is determined and used to design the MRAC adaptive law. The adaptive law used in the implementation of the standard MRAC can be derived as:

$$\dot{\hat{\theta}}_1^*=-\lambda_1 e\omega_1^*$$
$$\dot{\hat{\theta}}_2^*=-\lambda_2 e\omega_2^*$$

The associated robust MRAC adaptive laws are therefore given in equations (15) and (16). Equation (15) is the projection operator based MRAC and equation (16) is the dead zone based MRAC.

$$\dot{\hat{\theta}}_i^*=\begin{cases}\lambda_i e\omega_i^* & if\left|\hat{\theta}_i^*\right|<r_i, if\left|\hat{\theta}_i^*\right|=r_i.and.\hat{\theta}_i^* e\omega_i^*\le 0\\ 0 & if\left|\hat{\theta}_i^*\right|=r_i.and.\hat{\theta}_i^* e\omega_i^*>0\end{cases} \qquad i=1,2 \tag{15}$$

$$\dot{\hat{\theta}}_i^*=\begin{cases}\lambda_i e\omega_i^* & |e|>c\\ 0 & |e|\le c\end{cases} \qquad i=1,2 \tag{16}$$

4. Simulation Results and Analysis

This section shows the simulation results and by extension, the verification of the methods espoused in the earlier section. Simulation was performed in PLECS 4.5.6. Table 1 provides values of parameters used in the simulation. It commences with a comparative analysis of parameters $\hat{\theta}_1^*$ and $\hat{\theta}_2^*$ when the standard MRAC, projector operator based MRAC, and the dead zone based MRAC are applied. Figures 6 and 7 show parameters $\hat{\theta}_1^*$ and $\hat{\theta}_2^*$ respectively, with results showing that the standard MRAC parameters experience drift in parameters while the other two modified MRAC stop the parameter from drifting. The dead zone based MRAC is seen to work better at stopping the parameter drift phenomenon than the projection operator based MRAC. Hence for the basis of ensuring robustness to unmodelled ripples and measurement noise in the DAB, the dead zone MRAC is better. Based on this conclusion, further analysis was done on the dead zone based MRAC.

To implement the control techniques, the continuous time version of the controls were discretized using the Forward Euler method in a C-SCRIPT of the PLECS environment. So equation (16) was transformed to equation (17) noting that this equation loses its second term when $|\varepsilon|\le c$ and ΔT is the sampling time.

$$\begin{aligned}\hat{\theta}_1^*[k+1]&=\hat{\theta}_1^*[k]+\Delta T\left(\lambda_1 e[k]\omega_1^*[k]\right)\\ \hat{\theta}_2^*[k+1]&=\hat{\theta}_2^*[k]+\Delta T\left(\lambda_2 e[k]\omega_2^*[k]\right)\end{aligned} \tag{17}$$

Table 1. Parameters used in simulation

Symbol	Parameter	Units	Values
f_s	Switching frequency	kHz	20
L	Inductance	μH	70
N	Transformer turns ratio		2:1
C_2	DC capacitor at the output	mF	1
R_L	Load resistor	Ω	4

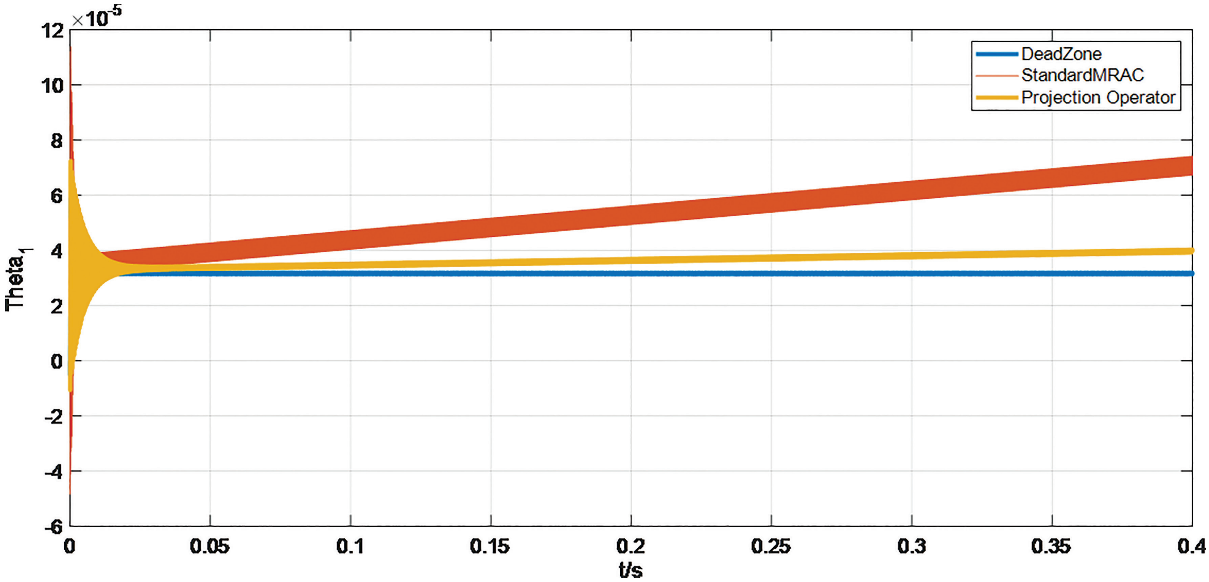

Figure 6. Parameter drift for $\hat{\theta}_1^*$ under standard MRAC and two other Robust MRAC.

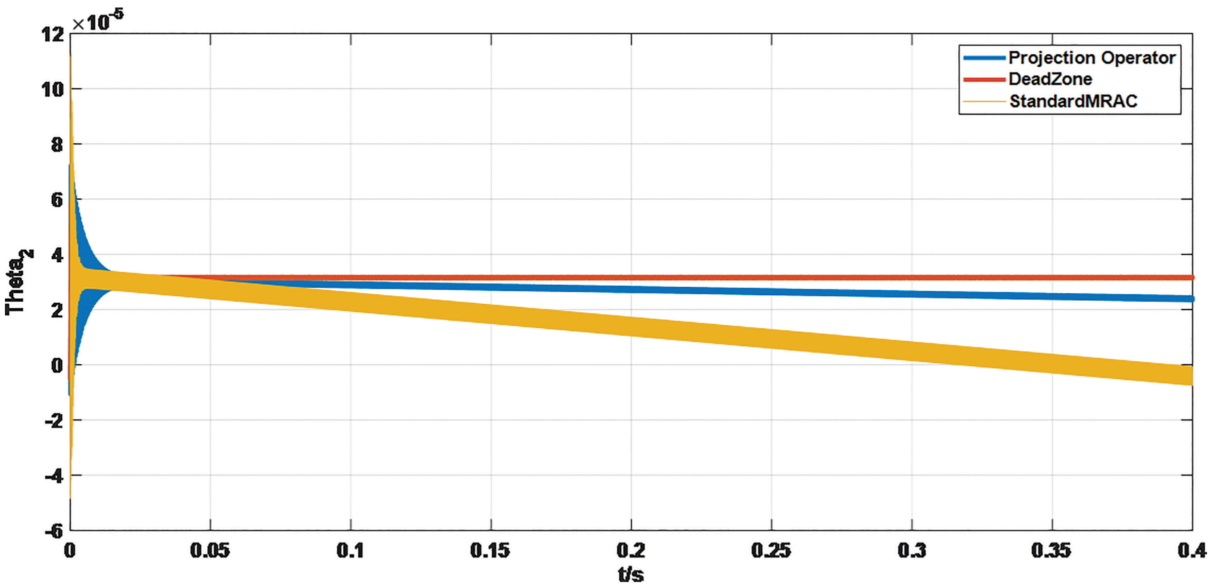

Figure 7. Parameter drift for $\hat{\theta}_2^*$ under standard MRAC and two other Robust MRAC.

This technique guaranteed, as illustrated in Figures 6 and 7, the stopping of adaptation when the parameters $\left(\hat{\theta}_1^*,\hat{\theta}_2^*\right)$ enter the dead zone. Consequently, it offered robustness against ripples and measurement noise, which the standard MRAC lacked. The robustness however compromised the performance of the voltage output in terms of increased overshoots. This was expected as learning was curtailed in the dead zone.

The dead zone technique was therefore further modified as follows:

If $|\varepsilon| \le c$ then $\hat{\theta}_i^*[k+1] = \alpha\hat{\theta}_i^*[k]$, where $0.5 \le \alpha \le 1$. The value of α was determined heuristically through several simulations. Figures 8 and 9 show the impact that changes in α had on the trajectory of the parameters as it was varied. In the legends of the relevant figures, signals labelled D1 denote designs and outputs related to the standard MRAC, while D2 pertains to designs and outputs of traditional dead zone. D3 and D4 are associated with the modified dead zone so adjusted such that $\alpha = 0.95$ and $\alpha = 0.5$ respectively. Generally, the traditional dead zone based MRAC has the lowest peaks recorded and longer duration (6 ms) before adaptation stops, modified dead zone with $\alpha = 0.5$ recorded the highest peak but shorter duration compared to D1 (2ms). The modified dead zone

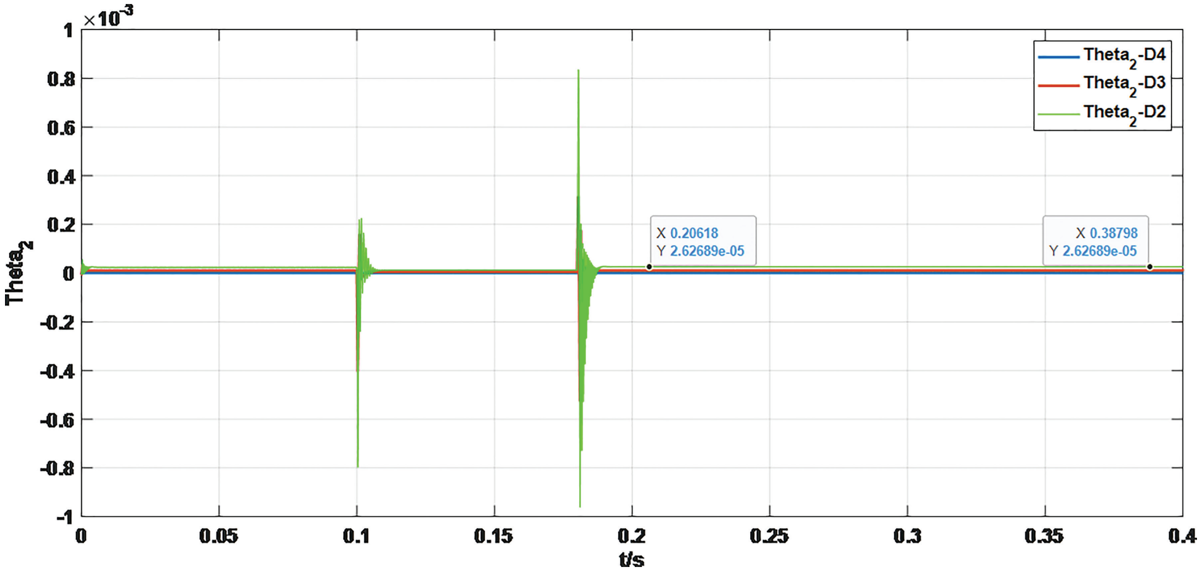

Figure 8. Parameter drift for $\hat{\theta}_2^*$ of traditional Dead Zone based MRAC and other modified Dead Zone based MRAC.

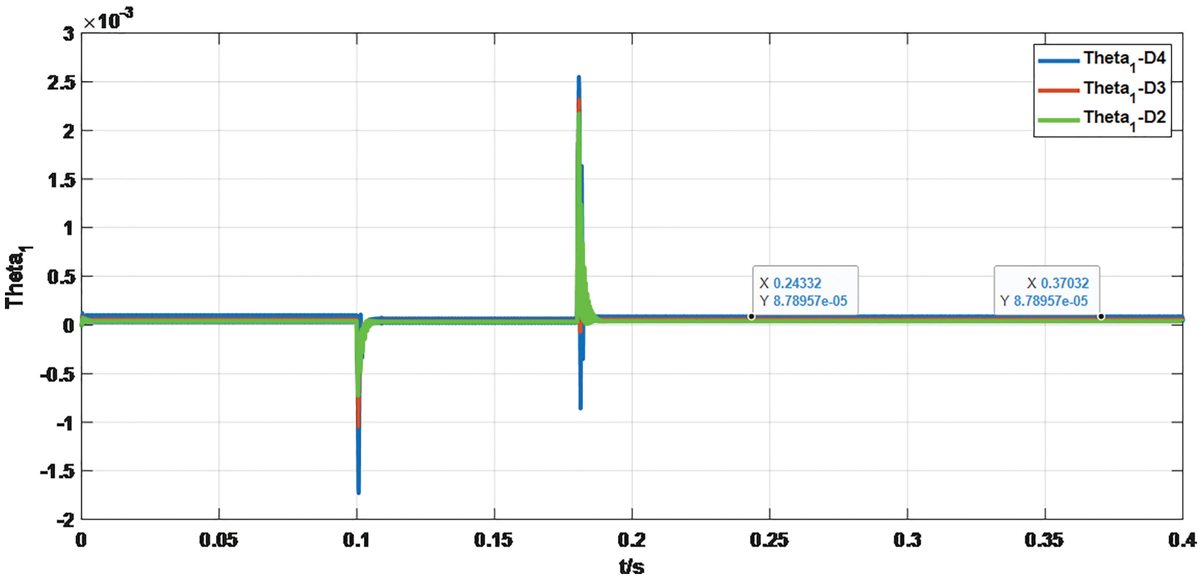

Figure 9. Parameter drift for $\hat{\theta}_1^*$ of traditional Dead Zone based MRAC and other modified Dead Zone based MRAC.

with $\alpha = 0.95$ recorded the fastest stopping of adaptation (under 1ms). Figure 10 shows a zoomed-in portion of Figure 8 to corroborate the observations.

The impact of the modification of the traditional dead zone based MRAC can also be seen in the performance of the output voltage v_2 of the DAB with CPL in Figures 11 and 12, with Figure 12 being an expanded version of Figure 11. Figure 11 records the trajectory of bus (output) voltage as techniques are varied. Nominal voltage values of v_1 and v_2 are 400v and 200v respectively. It is noted that within the 400ms time, output voltage is changed three times (160v, 100v and then to 170v). It can be observed that whereas all techniques guarantee stability and good tracking of the reference voltage, two present undesirable overshoots- standard MRAC (D1) and the traditional dead zone. However, these two on the contrary present lower steady state error compared to the other modified versions of the dead zone technology, with the standard MRAC(D1) recording almost zero steady state error. Again, it was realised that the lower values of α produced higher steady state errors as seen in Figure 12. This meant that the dead zone technique generally causes steady state gain errors, and its modified version further increases

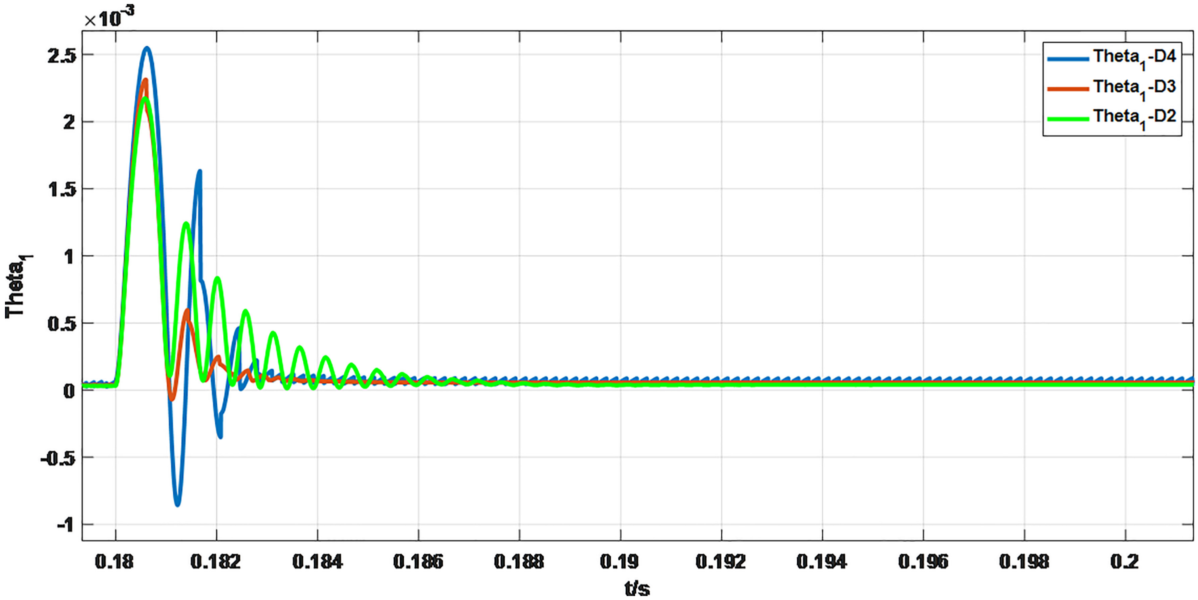

Figure 10. Enlarged version of portion of Figure 9.

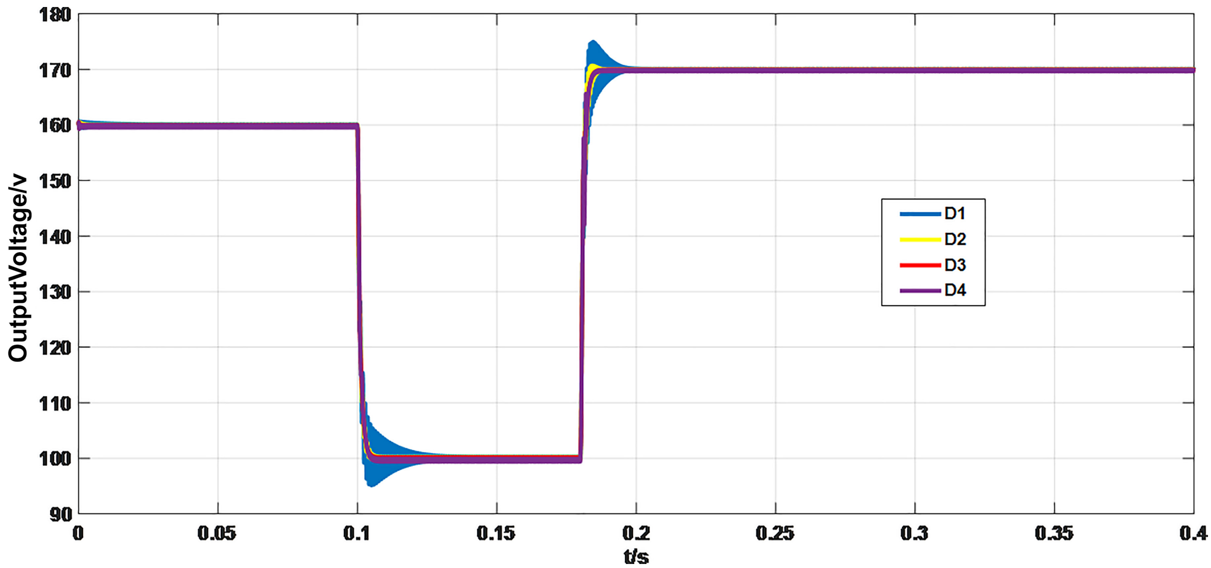

Figure 11. Output voltage of DAB as dead zone based MRAC design is varied.

the error. Beyond this finding, it was then decided that given the excellent tracking with no overshoot and minimal steady state error (0.16), the modified version of the dead zone with $\alpha = 0.95$ (D3) would be used in finalizing the design.

A further investigation into the impact of the adaptive gain on the modified dead zone based MRAC design was then undertaken. It was realized that tweaking the adaptive gains had an effect on the steady state error of the output voltage particularly, increasing the gain decreased the steady state error as evident in Figures 13 and 14. It was noticed that increasing the adaptive gains from 0.05 to 0.5 reduced the steady state errors from 0.1 to 0. The impact of the reference model (a_m) can also be observed in Figure 15, as anticipated, increasing a_m increased the dynamics of the output voltage only without the introduction of undesirable overshoots. As a result, after the design of the modified dead zone based MRAC, the adaptive gains can be fine-tuned to improve the steady state error and then the reference model parameter can also be tuned to improve the dynamic responses.

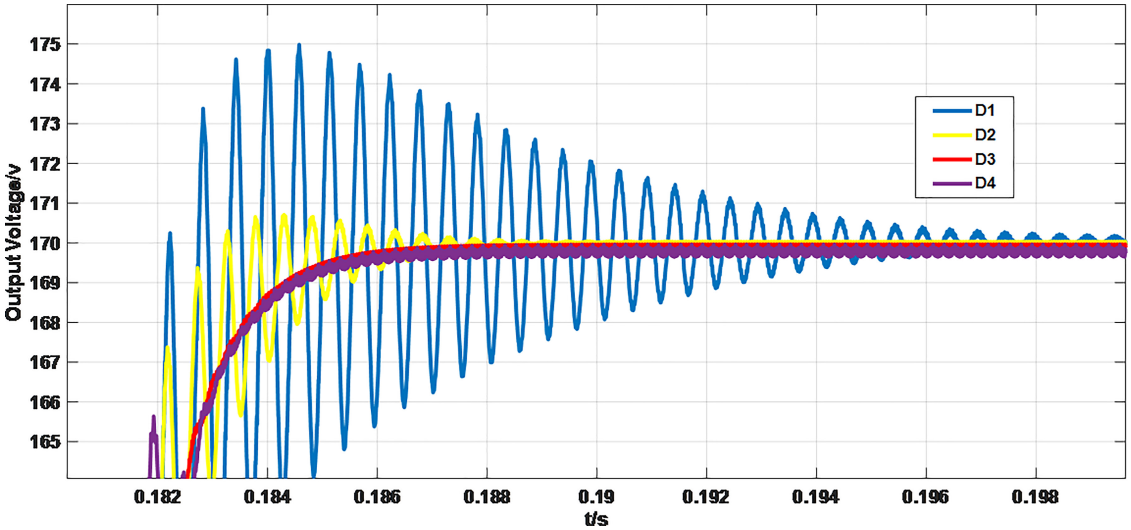

Figure 12. Enlarged portion of figure 11.

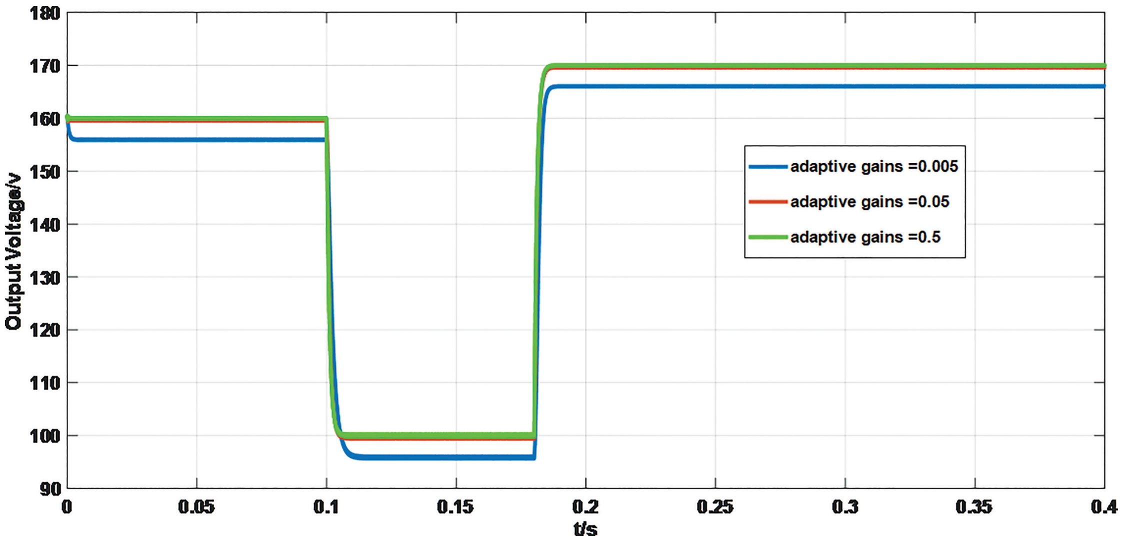

Figure 13. Impact of adaptive gains on the modified Dead Zone Based MRAC.

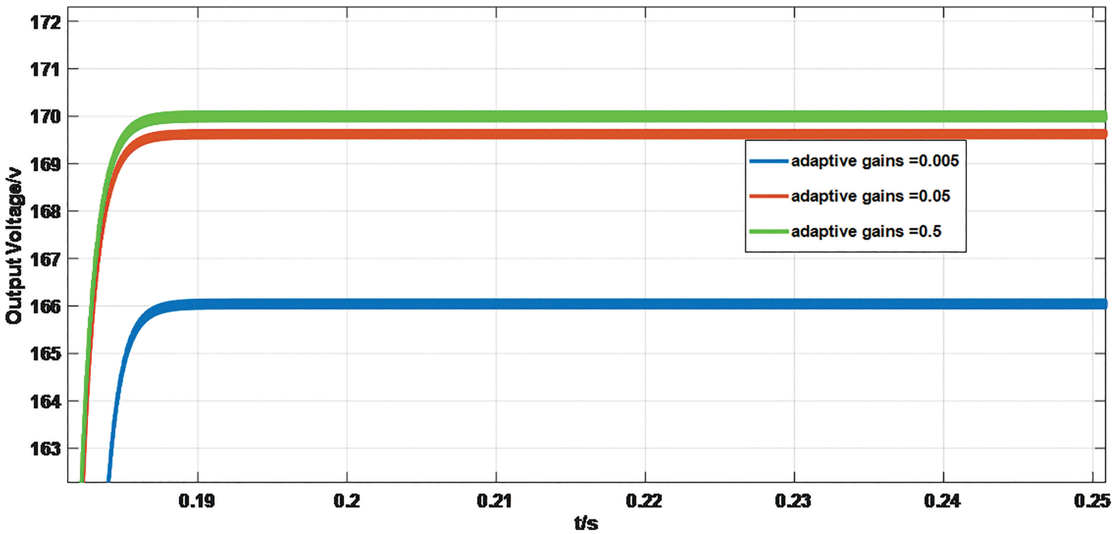

Figure 14. Enlargement of portion of Figure 13.

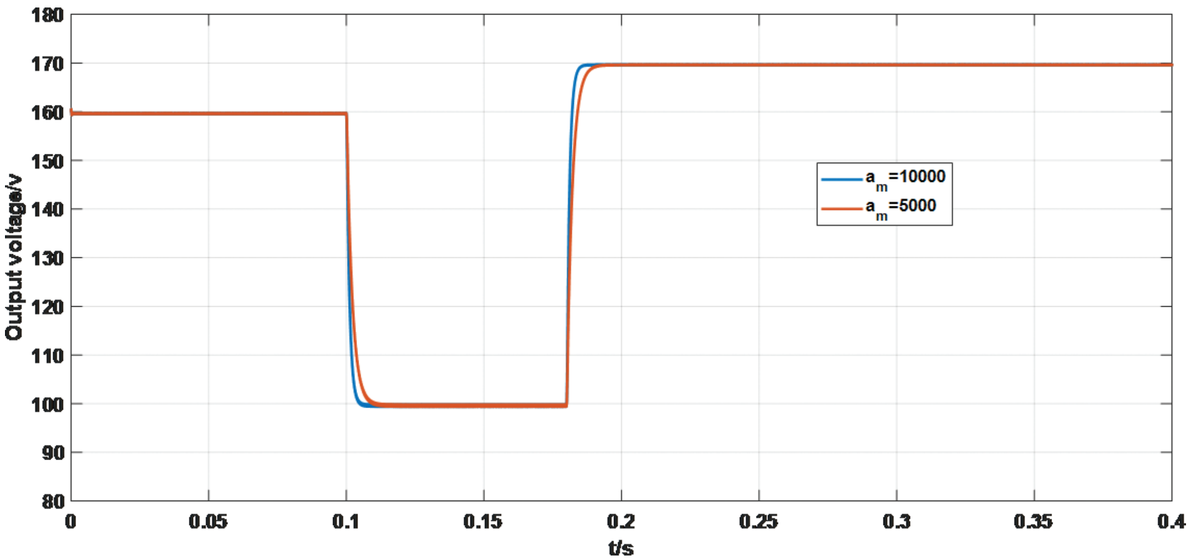

Figure 15. Impact of a_m on the modified Dead Zone based MRAC.

5. Conclusion

This paper introduced a modified version of the dead zone-based Model Reference Adaptive Control (MRAC) designed for Dual Active Bridge (DAB) converters with constant power loading (CPL). The proposed controller demonstrated significant improvements in preventing parameter drift when the control system is subjected to non-parametric uncertainties. It also maintains excellent performance in both dynamic and steady-state conditions of the DAB output voltage.

Tuning guidelines for the modified controller were developed based on simulation results, providing practical insights to ensure effective implementation. The paper also included a detailed analysis of the stability and convergence of the DAB control system, comparing the performance of standard MRAC, projection operator based MRAC, and dead zone techniques under non-parametric uncertainties. The results showed that while the projection operator technique offered some robustness benefits, the standard dead zone method was more effective in stopping parameter drift.

References

Brando, G., Del Pizzo, A. and Meo, S. (2018) 'Model-Reference Adaptive Control of a Dual Active Bridge DC-DC Converter for Aircraft Applications', *SPEEDAM 2018 - Proceedings: International Symposium on Power Electronics, Electrical Drives, Automation and Motion*, pp. 502–506. Available at: https://doi.org/10.1109/SPEEDAM.2018.8445242.

Chen, L., Shao, S., *et al.* (2020) 'Model Predictive Control for Dual-Active-Bridge Converters Supplying Pulsed Power Loads in Naval DC Micro-Grids', *IEEE Transactions on Power Electronics*, 35(2), pp. 1957–1966. Available at: https://doi.org/10.1109/TPEL.2019.2917450.

Chen, L., Lin, L., *et al.* (2020) 'Moving discretized control set model-predictive control for dual-active bridge with the triple-phase shift', *IEEE Transactions on Power Electronics*, 35(8), pp. 8624–8637. Available at: https://doi.org/10.1109/TPEL.2019.2962838.

Ding, Zhengtao. (2013) *Nonlinear and adaptive control systems*. Croydon: The Institution of Engineering and Technology.

Effah, E.K. *et al.* (2024) 'Model Reference Adaptive Control of SPS-Based Dual Active Bridge Converter with Constant Power Loading', *Power Electronics and Drives (sciendo)*, 9(44), pp. 348–357. Available at: https://doi.org/10.2478/pead-2024-0022.

He, J. *et al.* (2023) 'Review of Modeling, Modulation, and Control Strategies for the Dual-Active-Bridge DC/DC Converter', *Energies*, 16(18). Available at: https://doi.org/10.3390/en16186646.

Iqbal, M.T. *et al.* (2020) 'Explicit discrete modelling of bidirectional dual active bridge dc-dc converter using multi-time scale mixed system model', *IET Power Electronics*, 13(18), pp. 4252–4260. Available at: https://doi.org/10.1049/iet-pel.2020.0293.

Iyer, V.M., Gulur, S. and Bhattacharya, S. (2019) 'Small-signal stability assessment and active stabilization of a bidirectional battery charger', *IEEE Transactions on Industry Applications*, 55(1), pp. 563–574. Available at: https://doi.org/10.1109/TIA.2018.2871101.

Jeung, Y.C. and Lee, D.C. (2019) 'Voltage and current regulations of bidirectional isolated dual-active-bridge DC-DC converters based on a double-integral sliding mode control', *IEEE Transactions on Power Electronics*, 34(7), pp. 6937–6946. Available at: https://doi.org/10.1109/TPEL.2018.2873834.

Meng, X. *et al.* (2023) 'A Novel Intelligent Nonlinear Controller for Dual Active Bridge Converter With Constant Power Loads', *IEEE Transactions on Industrial Electronics*, 70(3), pp. 2887–2896. Available at: https://doi.org/10.1109/TIE.2022.3170608.

Mueller, J.A. and Kimball, J.W. (2018) 'An Improved Generalized Average Model of DC-DC Dual Active Bridge Converters', *IEEE Transactions on Power Electronics*, 33(11), pp. 9975–9988. Available at: https://doi.org/10.1109/TPEL.2018.2797966.

Rahimi, A.M. and Emadi, A. (2009) 'Active damping in DC/DC power electronic converters: A novel method to overcome the problems of constant power loads', *IEEE Transactions on Industrial Electronics*, 56(5), pp. 1428–1439. Available at: https://doi.org/10.1109/TIE.2009.2013748.

Shah, S.S. and Bhattacharya, S. (2017) 'Large & small signal modeling of dual active bridge converter using improved first harmonic approximation', *Conference Proceedings - IEEE Applied Power Electronics Conference and Exposition - APEC*, pp. 1175–1182. Available at: https://doi.org/10.1109/APEC.2017.7930844.

Shao, S. *et al.* (2022) 'Modeling and Advanced Control of Dual-Active-Bridge DC-DC Converters: A Review', *IEEE Transactions on Power Electronics*, 37(2), pp. 1524–1547. Available at: https://doi.org/10.1109/TPEL.2021.3108157.

Wu, M. and Lu, D.D.C. (2015) 'A Novel Stabilization Method of LC Input Filter with Constant Power Loads Without Load Performance Compromise in DC Microgrids', *IEEE Transactions on Industrial Electronics*, 62(7), pp. 4552–4562. Available at: https://doi.org/10.1109/TIE.2014.2367005.

Xiao, Q. *et al.* (2020) 'Model Predictive Control for Dual Active Bridge in Naval DC Microgrids Supplying Pulsed Power Loads Featuring Fast Transition and Online Transformer Current Minimization', *IEEE Transactions on Industrial Electronics*, 67(6), pp. 5197–5203. Available at: https://doi.org/10.1109/TIE.2019.2934070.